



**HAL**  
open science

## **Autoradiography validation of novel tau PET tracer [F-18]-MK-6240 on human postmortem brain tissue**

Cinthy Aguero, Maeva Dhaynaut, Marc D Normandin, Ana C Amaral, Nicolas J Guehl, Ramesh Neelamegam, Marta Marquie, Keith Johnson, Georges El Fakhri, Georges El Fakhri, et al.

### ► **To cite this version:**

Cinthy Aguero, Maeva Dhaynaut, Marc D Normandin, Ana C Amaral, Nicolas J Guehl, et al.. Autoradiography validation of novel tau PET tracer [F-18]-MK-6240 on human postmortem brain tissue. *Acta Neuropathologica Communications*, 2019, 7, pp.37. 10.1186/s40478-019-0686-6 . hal-02083601

**HAL Id: hal-02083601**

**<https://hal.sorbonne-universite.fr/hal-02083601>**

Submitted on 29 Mar 2019

**HAL** is a multi-disciplinary open access archive for the deposit and dissemination of scientific research documents, whether they are published or not. The documents may come from teaching and research institutions in France or abroad, or from public or private research centers.


L'archive ouverte pluridisciplinaire **HAL**, est destinée au dépôt et à la diffusion de documents scientifiques de niveau recherche, publiés ou non, émanant des établissements d'enseignement et de recherche français ou étrangers, des laboratoires publics ou privés.

RESEARCH

Open Access



# Autoradiography validation of novel tau PET tracer [F-18]-MK-6240 on human postmortem brain tissue

Cintha Aguero<sup>1,2</sup>, Maeva Dhaynaut<sup>3,4</sup>, Marc D. Normandin<sup>3</sup>, Ana C. Amaral<sup>1,2</sup>, Nicolas J. Guehl<sup>3</sup>, Ramesh Neelamegam<sup>3</sup>, Marta Marquie<sup>1,2</sup>, Keith A. Johnson<sup>5</sup>, Georges El Fakhri<sup>3</sup>, Matthew P. Frosch<sup>2,6</sup> and Teresa Gomez-Isla<sup>1,2\*</sup> 

## Abstract

[F-18]-MK-6240, a novel tau positron emission tomography (PET) tracer recently discovered for the in vivo detection of neurofibrillary tangles, has the potential to improve diagnostic accuracy in the detection of Alzheimer disease. We have examined regional and substrate-specific binding patterns as well as possible off-target binding of this tracer on human brain tissue to advance towards its validation. We applied [F-18]-MK-6240 phosphor screen and high resolution autoradiography to postmortem samples from patients with a definite pathological diagnosis of Alzheimer disease, frontotemporal lobar degeneration-tau (Pick's disease, progressive supranuclear palsy and corticobasal degeneration), chronic traumatic encephalopathy, frontotemporal lobar degeneration-Tar DNA-binding protein 43 (TDP-43), dementia with Lewy bodies, cerebral amyloid angiopathy and elderly controls free of pathologic changes of neurodegenerative disease. We also directly compared the binding properties of [F-18]-MK-6240 and [F-18]-AV-1451 in human tissue, and examined potential nonspecific binding of both tau tracers to monoamine oxidases (MAO) by using autoradiography in the presence of selective monoamine oxidase A (MAO-A) and monoamine oxidase B (MAO-B) inhibitors. Our data indicate that MK-6240 strongly binds to neurofibrillary tangles in Alzheimer disease but does not seem to bind to a significant extent to tau aggregates in non-Alzheimer tauopathies, suggesting that it may have a limited utility for the in vivo detection of these pathologies. There is no evidence of binding to lesions containing  $\beta$ -amyloid,  $\alpha$ -synuclein or TDP-43. In addition, we identified MK-6240 strong off-target binding to neuromelanin and melanin-containing cells, and some weaker binding to areas of hemorrhage. These binding patterns are nearly identical to those previously reported by our group and others for [F-18]-AV-1451. Of note, [F-18]-MK-6240 and [F-18]-AV-1451 autoradiographic binding signals were only weakly displaced by competing concentrations of selective MAO-B inhibitor deprenyl but not by MAO-A inhibitor clorgyline, suggesting that MAO enzymes do not appear to be a significant binding target of any of these two tracers. Together these novel findings provide relevant insights for the correct interpretation of in vivo [F-18]-MK-6240 PET imaging.

## Introduction

The recent development of several novel positron emission tomography (PET) tracers tailored to detect tau in the brain has opened the opportunity of using them to improve diagnostic accuracy in Alzheimer disease (AD) and related tauopathies, and to allow reliable quantification of

brain tau burden and tracking of disease progression by in vivo neuroimaging [15, 35].

Emerging data from early studies -including our own- on postmortem material with the most validated thus far, [F-18]-AV-1451 (T807, Flortaucipir), have shown that this ligand binds with strong affinity to paired helical filament (PHF)-tau aggregates in AD brains and those that form as a function of age [20–22, 27, 35], closely matching the stereotypical spatiotemporal progression of neurofibrillary tangles (NFT) as described by Braak [3]. In agreement with these observations, patients

\* Correspondence: [tgomezisla@mgh.harvard.edu](mailto:tgomezisla@mgh.harvard.edu)

<sup>1</sup>Department of Neurology, Massachusetts General Hospital, WACC, Suite 715, 15th Parkman St., Boston, MA 02114, USA

<sup>2</sup>MassGeneral Institute for Neurodegenerative Disease, Charlestown, MA, USA  
Full list of author information is available at the end of the article



clinically diagnosed with dementia of AD type and mild cognitive impairment (MCI) exhibit significantly higher in vivo [F-18]-AV-1451 retention than cognitively normal individuals in regions that are known to contain an elevated burden of tau lesions in AD [4, 6, 7, 11, 16, 25, 28, 33]. The overall utility of this tracer for in vivo selective and reliable detection of tau aggregates in non-AD tauopathies, however, seems very limited with the exception of certain tau mutations causing frontotemporal lobar degeneration (FTLD) characterized by tau aggregates [26] that contain all six isoforms of tau (three-repeat (3R) and four-repeat (4R)) [14] with PHF ultrastructure resembling NFT found in AD. We and others have shown that [F-18]-AV-1451 has low affinity for tau aggregates that contain primarily 4R tau with straight filament ultrastructure that predominate in tauopathies such as progressive supranuclear palsy (PSP), corticobasal degeneration (CBD), and most cases of FTLD. We also demonstrated the existence of robust [F-18]-AV-1451 off-target binding to melanin- and neuromelanin-containing cells and some weaker binding to blood components [21, 22]. Controversy exists as to whether AV-1451 may also exhibit significant nonspecific binding to MAO enzymes [12, 15, 17, 30], as it has been recently demonstrated for other tau PET tracers like THK-5351 [13, 24].

Several second-generation tau tracers have more recently been reported. The one that has garnered most attention and is largely considered to have most promise is [F-18]-MK-6240 from the Merck Translational Biomarkers team [15, 32]. To date, very limited information is available about the binding properties of this tracer. Merck's researchers performed in vitro binding screens against a wide panel of known receptor, transporter, and enzyme targets but conducted only limited autoradiography studies on AD and control brain specimens [15]. Yet, this ligand is quickly making its way into observational studies and clinical trials. Thus, a comprehensive postmortem validation of MK-6240 is critical for determining its usefulness for antemortem diagnosis and staging of AD and other tauopathies, and to understand exactly what [F-18]-MK-6240 PET positivity means in terms of neuropathological substrate. Because MK-6240 was initially screened in vitro for NFT binding affinity using AD brain homogenates rich in NFT and an amyloid plaque tracer for counterscreening [15], and seemed to bind to the same site as AV-1451 in that tissue material, we predicted that, just like AV-1451, MK-6240 would exhibit high binding affinity and selectivity for PHF-tau lesions relative to non-PHF-tau lesions, A $\beta$  deposits and  $\alpha$ -synuclein and transactive response DNA binding protein-43 (TDP-43) aggregates.

To validate the site/s of MK-6240 binding and determine whether there is off-target binding, we examined

the regional and substrate-selective autoradiographic patterns of [F-18]-MK-6240 in postmortem brain, retina and skin tissue samples. Cases with a definite pathological diagnosis of AD, FTLD-tau (PiD, PSP, CBD), chronic traumatic encephalopathy (CTE), FTLD-TDP-43, dementia with Lewy bodies (DLB), cerebral amyloid angiopathy (CAA), metastatic melanoma, brain hemorrhages, and elderly controls free of neurodegenerative diseases were studied. Most of these cases had also been included in our previous validation studies of [F-18]-AV-1451 [21, 22], giving us the opportunity to directly compare the autoradiographic binding patterns of both tracers in comparable tissue samples.

## Materials and methods

### Tissue samples

Postmortem brain, retina and skin tissue samples from the Massachusetts and the Boston University Alzheimer's Disease Research Centers Neuropathology cores were included in this study. Autopsies were performed according to standardized protocol [31] and tissue collection and use was approved by the local Institutional Review Boards. A summary of the demographic characteristics of the cases studied is shown in Table 1.

Histological evaluation of each case was routinely performed on a specific set of 19 blocked regions representative for a spectrum of neurodegenerative diseases. All paraffin-embedded blocks were stained with Luxol fast blue and hematoxylin and eosin (LH&E), while selected blocks were routinely stained for Bielschowsky silver stain and A $\beta$ ,  $\alpha$ -synuclein, ubiquitin, TDP-43 and phospho-tau immunoreactivity. Blocks of frozen brain tissue containing hippocampal formation, entorhinal cortex (EC), frontal, parietal, temporal and occipital cortices, cerebellum, basal ganglia and midbrain were cut into sections 10  $\mu$ m-thick in a cryostat (Thermo-Shandon SME Cryostat), mounted on Histobond adhesion slides (StatLab, TX) and used for [F-18]-MK-6240 phosphor screen and nuclear emulsion high resolution autoradiography, followed by immunohistochemistry using appropriate antibodies in each case.

### [F-18]-MK-6240 phosphor screen autoradiography

[F-18]-MK-6240 was synthesized as previously described [8]. Autoradiography experiments were performed using [F-18]-MK-6240 aliquots from material prepared from in vivo imaging on the same day, and following our previously published protocol [22]. In brief, 10  $\mu$ m-thick frozen brain sections were fixed in 100% methanol at room temperature for 20 min and then transferred to a bath containing high specific activity [F-18]-MK-6240 in 10 mM PBS with a radioactivity concentration of approximately 10  $\mu$ Ci/ml. Adjacent brain slices were placed in a bath that was identical in all aspects except that

**Table 1** Participants' characteristics

ID#	Clinical diagnosis	Pathological diagnosis	Age at death (yrs)	Gender	PMI (hrs)	Braak & Braak (NFT)	CERAD score (neuritic plaques)	NIA-Reagan Institute criteria
#1	CTL	Normal adult brain	86	M	10	I	none	LP
#2	CTL	Normal adult brain	73	F	20	I	none	LP
#3	CTL	Normal adult brain	101	F	22	II	A	LP
#4	AD	AD	96	F	20	V	C	HP
#5	AD	AD	78	F	18	VI	C	HP
#6	AD	AD	97	F	12	VI	A	HP
#7	AD	AD	87	F	12	IV	B	IP
#8	AD	AD	60	M	24	VI	C	HP
#9	AD	AD	82	F	6	V	B	HP
#10	AD	AD	69	F	4	VI	C	HP
#11	AD	AD	70	M	6	V	C	HP
#12	AD	AD	66	F	2	VI	C	HP
#13	AD	AD	66	F	10	VI	C	HP
#14	AD	AD	97	F	24	V	C	HP
#15	AD	AD	81	M	7	IV	C	IP
#16	FTLD	AD/CAA	66	M	16	V	B	HP
#17	Memory, speech and gait difficulties, hand tremor	Diffuse CAA (D23N IowA APP mutation)	45	M	N/A	I	none	LP
#18	AD	AD/Metastatic melanoma	75	M	35	V	B	IP
#19	FTLD	PiD, type A	61	M	19	N/A	N/A	N/A
#20	FTLD	PiD	62	M	19	I	A	LP
#21	FTLD (P301L Mutation)	FTLD	71	F	4	I	none	LP
#22	FTLD	DLDH	65	M	24	I	none	LP
#23	CBD	CBD	80	M	6	I	none	LP
#24	PSP	PSP	69	M	45	II	none	LP
#25	PSP	PSP	68	M	48	II	none	LP
#26	PSP	PSP	78	M	11	II	none	LP
#27	PSP	PSP	73	M	12	II	none	LP
#28	PSP	PSP	63	F	12	II	none	LP
#29	CTE	CTE (CTE stage II-III) [23]	25	M	27	0	none	LP
#30	CTE	CTE (CTE stage III)	56	M	N/A	II	none	LP
#31	CTE	CTE (CTE stage III)	46	M	72	III	none	LP
#32	CTE	CTE (CTE stage IV)	65	M	N/A	II	A	LP
#33	CTE	CTE (CTE stage III)	58	M	N/A	III	none	LP
#34	DLB	LBD	62	M	24	N/A	none	N/A
#35	DLB	LBD, brainstem predominant	76	M	17	II	none	LP
#36	PDD	LBD (Braak stage 4/6)	83	M	9	III	none	LP
#37	MSA	MSA, cerebellar type (MSA-C)	60	F	32	II	none	LP
#38	FTLD	FTLD-TDP-43, type A	69	F	16	I	none	LP
#39	FTLD	FTLD-TDP-43	55	M	14	I	none	LP
#40	FTLD	FTLD-TDP-43	68	M	49	I	none	LP
#41	FTLD	FTLD-TDP-43	64	M	12	I	none	LP

**Table 1** Participants' characteristics (Continued)

ID#	Clinical diagnosis	Pathological diagnosis	Age at death (yrs)	Gender	PMI (hrs)	Braak & Braak (NFT)	CERAD score (neuritic plaques)	NIA-Reagan Institute criteria
#42	Headache	Subarachnoid hemorrhage	92	F	N/A	IV	A	IP
#43	N/A	Parenchymal hemorrhage	75	M	N/A	I	none	LP

*Abbreviations:* AD Alzheimer's disease, APP amyloid precursor protein, CAA Cerebral amyloid angiopathy, CBD Corticobasal degeneration, CERAD Consortium to establish a registry for Alzheimer's disease, CTL Control subject, DLB Dementia with lewy bodies, DLDH Dementia lacking distinctive histopathology, F Female, FTL D Frontotemporal lobar degeneration, HP High probability, IP Intermediate probability, LP Low probability, M Male, MSA Multiple systemic atrophy, NFT Neurofibrillary tangles, NIA National Institute of Aging, N/A Non available, PID Pick's disease, PMI Postmortem interval, PSP Progressive supranuclear palsy, TDP-43 TAR DNA binding protein 43

unlabeled MK-6240 was added to yield 500 nM chemical concentration, a blocking condition sufficient to saturate essentially all available specific binding sites of tau [35]. Additional adjacent slices were also incubated in separate baths containing either [F-18]-MK-6240 or [F-18]-AV-1451 with a radioactivity concentration of approximately 10 µCi/ml and 20 µCi/ml respectively, and selective MAO-A (clorgyline) and MAO-B (deprenyl) inhibitors (Sigma-Aldrich) were added at a competing concentration of 1 µM to evaluate potential displacement of [F-18]-MK-6240 and [F-18]-AV-1451 binding signals. After incubation for 60 min, racks of slides were removed from the respective radioactive solutions and briefly incubated in a series of wash baths to remove unbound radiotracer. Wash solutions and incubation times were: 10 mM PBS for 1 min, 70% ethanol/30% PBS for 2 min, 30% ethanol/70% PBS for 1 min, and lastly 100% 10 mM PBS for 1 min. Racks were removed from the final wash solution and slices were allowed to air dry before transfer of the slides to a storage phosphor screen (MultiSensitive Phosphor Screen, PerkinElmer Life and Analytic Sciences, Shelton, CT) that had been photo-bleached immediately prior by exposure on a white light box for a minimum of 15 min. The slides and phosphor screen were enclosed in an aluminum film cassette and set in a dark area away from sources of radioactivity for the duration of the overnight exposure period. Under dim lighting conditions, the cassette was opened and the slides removed from the exposed screen, which was mounted to the carousel of the digital imaging system (Cyclone Plus Storage Phosphor Scanner, PerkinElmer Life and Analytic Sciences). Scanning of screens was controlled by the manufacturer's OptiQuant software package using the highest available resolution of 600 dpi (approximately 42 µm sampling interval). Digital images were saved in uncompressed form at full resolution and pixel depth. Images from adjacent brain slices incubated in the unblocked (high specific activity [F-18]-MK-6240 only) and blocking ([F-18]-MK-6240 plus 500 nM unlabeled MK-6240) conditions were compared to determine total and non-specific binding of [F-18]-MK-6240 in the tissue.

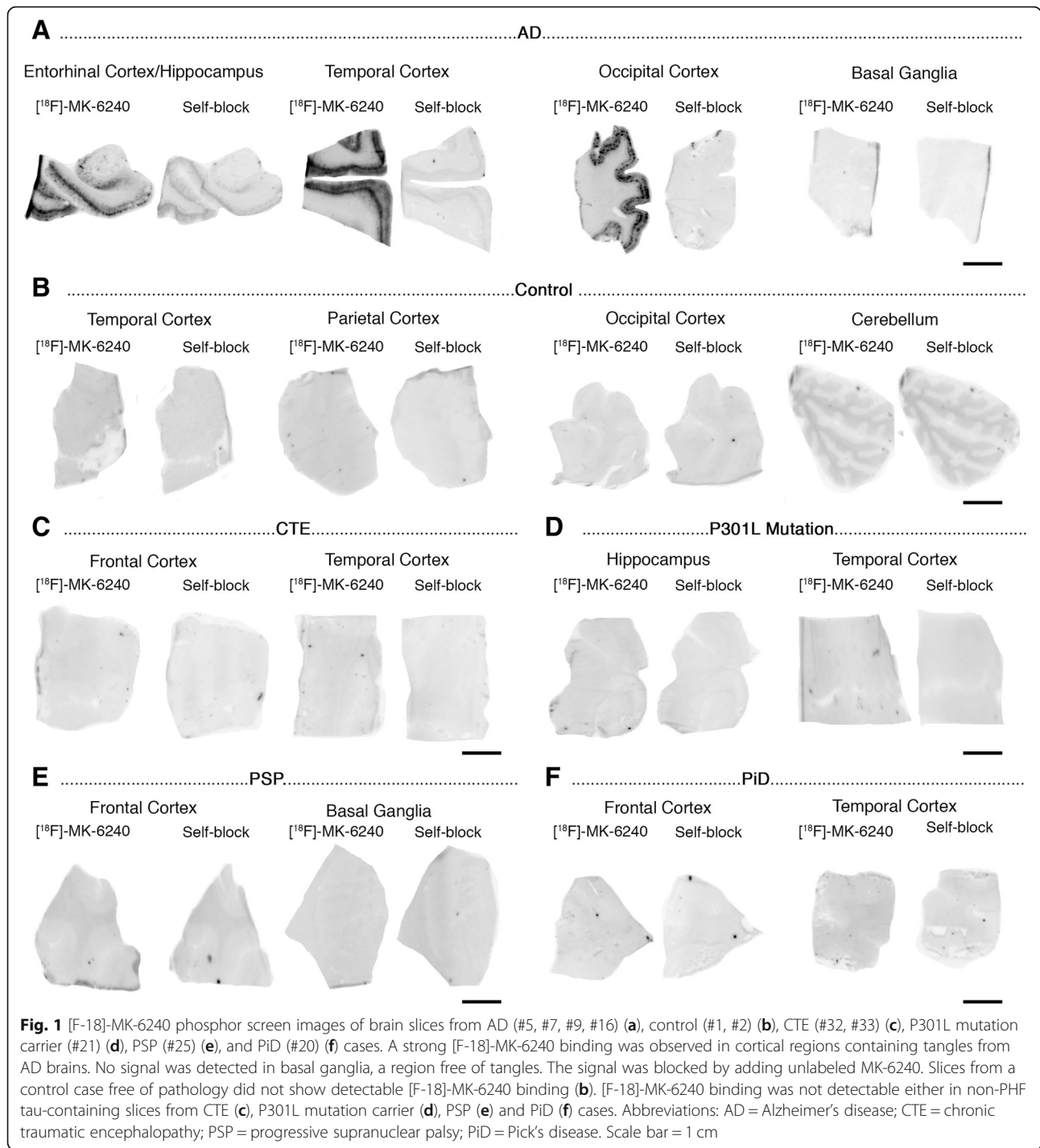
**[F-18]-MK-6240 high resolution nuclear emulsion autoradiography and immunohistochemistry**

To obtain autoradiographic information at the cellular resolution level, frozen cryostat sections, adjacent to those used for phosphor screen autoradiography, were coated with a liquid photographic emulsion following our previously published protocol [5, 9, 22, 34]. Immunohistochemistry was then performed on the nuclear emulsion-dipped sections. First the sections were washed for 5 min with PBS, then incubated with 2.5% normal horse blocking serum for 20 min, followed by the appropriate primary antibody - anti-tau PHF-1 (1:100, mouse, kind gift of Dr. Peter Davies), anti-Aβ (1:500, mouse, clone 6F/3D, Dako), anti α-synuclein (1:100, mouse, Zymed) or anti-phospho TDP-43 (pS409/410) (1:3000, mouse, Cosmo Bio CO) - for 40 min at 37 °C, washed with PBS twice for 2 min, and then incubated with the secondary antibody (ImmPRESS™ anti-mouse IgG (Vector Laboratories product MP-2400, Burlingame, CA) or ImmPRESS™ anti-rabbit Ig (Vector Laboratories product MP-7401, Burlingame, CA)) for 40 min at 37 °C. The sections were washed again with PBS twice for 2 min, and developed with DAB solution (Vector Laboratories product SK-4100). H&E was used for counterstaining. Photomicrographs were obtained on an upright Olympus BX51 (Olympus, Denmark) microscope using visible light.

**Results**

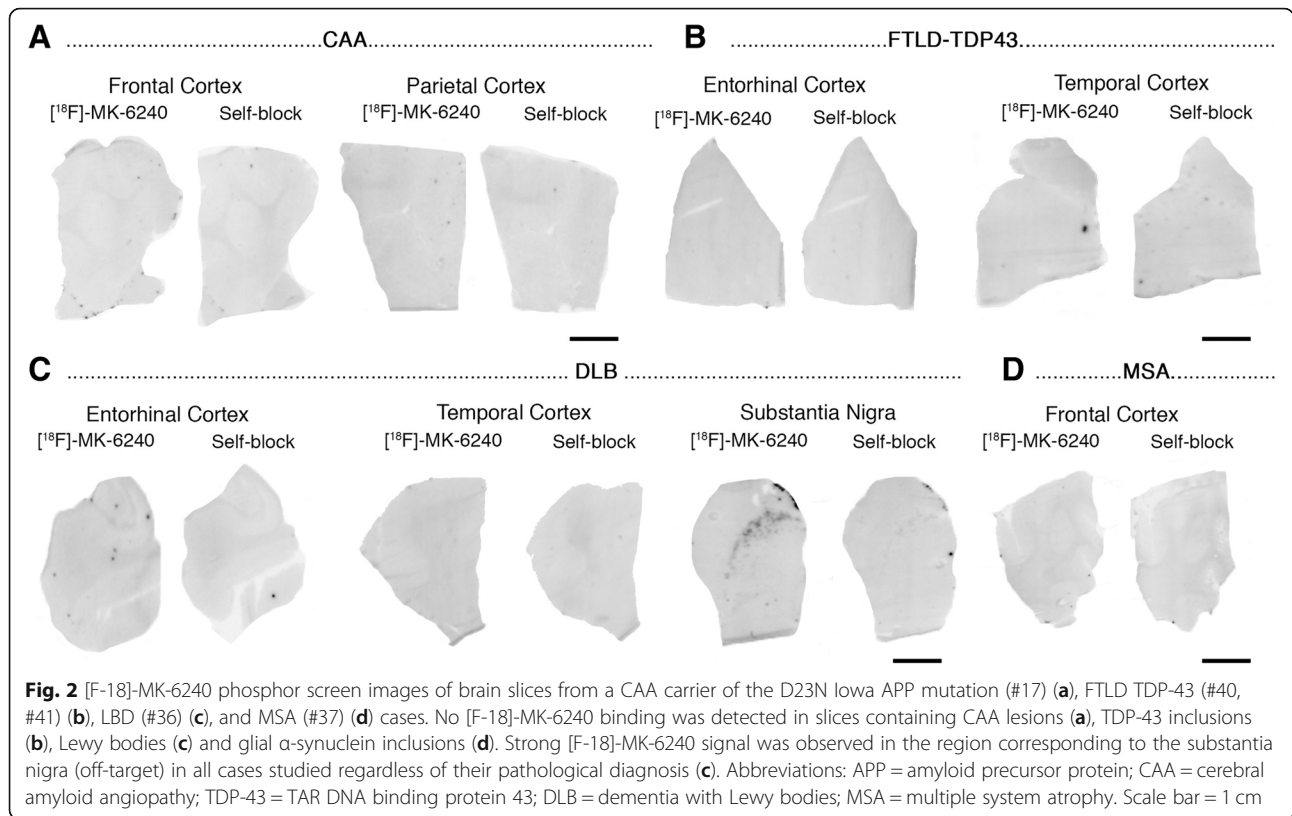
**[F-18]-MK-6240 phosphor screen autoradiography**

Phosphor screen autoradiography experiments revealed strong binding of [F-18]-MK-6240 in the hippocampal formation/EC and frontal, temporal, parietal and occipital cortices from brain slices containing NFT in AD cases (Fig. 1a). This binding was blocked after incubating the slides with 500 nM unlabeled MK-6240, demonstrating the selectivity of the signal. No binding was detected in non-tangle containing cortical regions or in the white matter in AD and control cases (Fig. 1b). MK-6240 binding was also absent in the cerebellum - typically used in neuroimaging studies as a reference region and lacking tangles in AD - and in the basal ganglia (Fig. 1a-f) of all



the cases studied in this series. Of note, no detectable MK-6240 binding could be observed in brain slices containing non-PHF tau aggregates from PiD, PSP, CBD and CTE cases (Fig. 1c, e-f) or in a *MAPT*P301L mutation carrier (Fig. 1d). This favors the idea that MK-6240 binds with significantly stronger affinity and selectivity to tau aggregates containing all six isoforms of tau (3R and 4R) with paired helical filament (PHF) ultrastructure

than to tau lesions primarily made of either 3R or 4R isoforms with straight filament ultrastructure. Brain slices from a D23N Iowa APP mutation carrier [29] displaying very severe CAA but no tau aggregates completely lacked [<sup>18</sup>F]-MK-6240 autoradiographic signal (Fig. 2a) and were indistinguishable from control brain slices. Brain slices containing TDP-43 inclusions in FTL-D-TDP-43 cases (Fig. 2b) and α-synuclein lesions in



DLB (Fig. 2c) and MSA (Fig. 2d) cases also lacked detectable [<sup>18</sup>F]-MK-6240 binding. A strong off-target binding of [<sup>18</sup>F]-MK-6240 was present in midbrain slices containing substantia nigra in all samples examined, regardless of the presence or absence of tau aggregates; this signal was blocked almost completely when incubating the slides with 500 nM unlabeled MK-6240 (Fig. 3a). In addition, [<sup>18</sup>F]-MK-6240 off-target binding was also noticed in retinal pigment epithelium, brain metastatic melanoma, brain slices containing parenchymal hemorrhages and extracutaneous meningeal melanocytes (Fig. 3b-f).

Overall, the [<sup>18</sup>F]-MK-6240 autoradiographic specific and off-target binding patterns described above are comparable to those exhibited by [<sup>18</sup>F]-AV-1451 that we and others have previously described in detail elsewhere [22]. Of note, [<sup>18</sup>F]-MK-6240 binding was blocked after incubating the slides with 500 nM unlabeled AV-1451 and vice versa (Fig. 4).

Importantly, when a competing concentration of 1 μM clorgyline (a selective MAO-A inhibitor) was added to the blocking solution, neither [<sup>18</sup>F]-MK-6240 nor [<sup>18</sup>F]-AV-1451 autoradiographic signal displacement could be detected (Fig. 5). [<sup>18</sup>F]-MK-6240 and [<sup>18</sup>F]-AV-1451 binding signals were only very weakly displaced (by about 20%) with 1 μM deprenyl (a selective MAO-B inhibitor) (Fig. 5), pointing to MAO-B as a low binding affinity site of these two tracers.

#### [<sup>18</sup>F]-MK-6240 high resolution nuclear emulsion autoradiography and immunohistochemistry

With the purpose of obtaining enough resolution at the cellular level, we dipped adjacent brain slices to those used in phosphor screen autoradiography in a photographic nuclear emulsion. Once the slides are developed, the visualization of silver grains struck by positrons emitted during [<sup>18</sup>F] nuclear decay enables precise identification of [<sup>18</sup>F]-MK-6240 labeled lesions by optical microscopy.

Using this method, we confirmed the presence of a strong and selective concentration of silver grains in tissue sections from AD cases, reflecting underlying [<sup>18</sup>F]-MK-6240 binding in the NFT-containing grey matter with negligible presence of silver grains in the white matter and following a very similar pattern to that observed with [<sup>18</sup>F]-AV-1451 (Fig. 6a-b). The silver grain distribution in the hippocampal formation/EC, and frontal, parietal, temporal and occipital cortices in AD brains closely matched the laminar distribution of tangles on adjacent slices as revealed by PHF-1 immunostaining rather than the more scattered plaque distribution pattern revealed by Aβ immunostaining (Fig. 6a-b). Silver grains were particularly abundant in layers III and V of association cortex (Fig. 6a-b) and layers II and IV in the entorhinal cortex (Fig. 6c), matching the well known laminar pattern of NFT in AD [1,

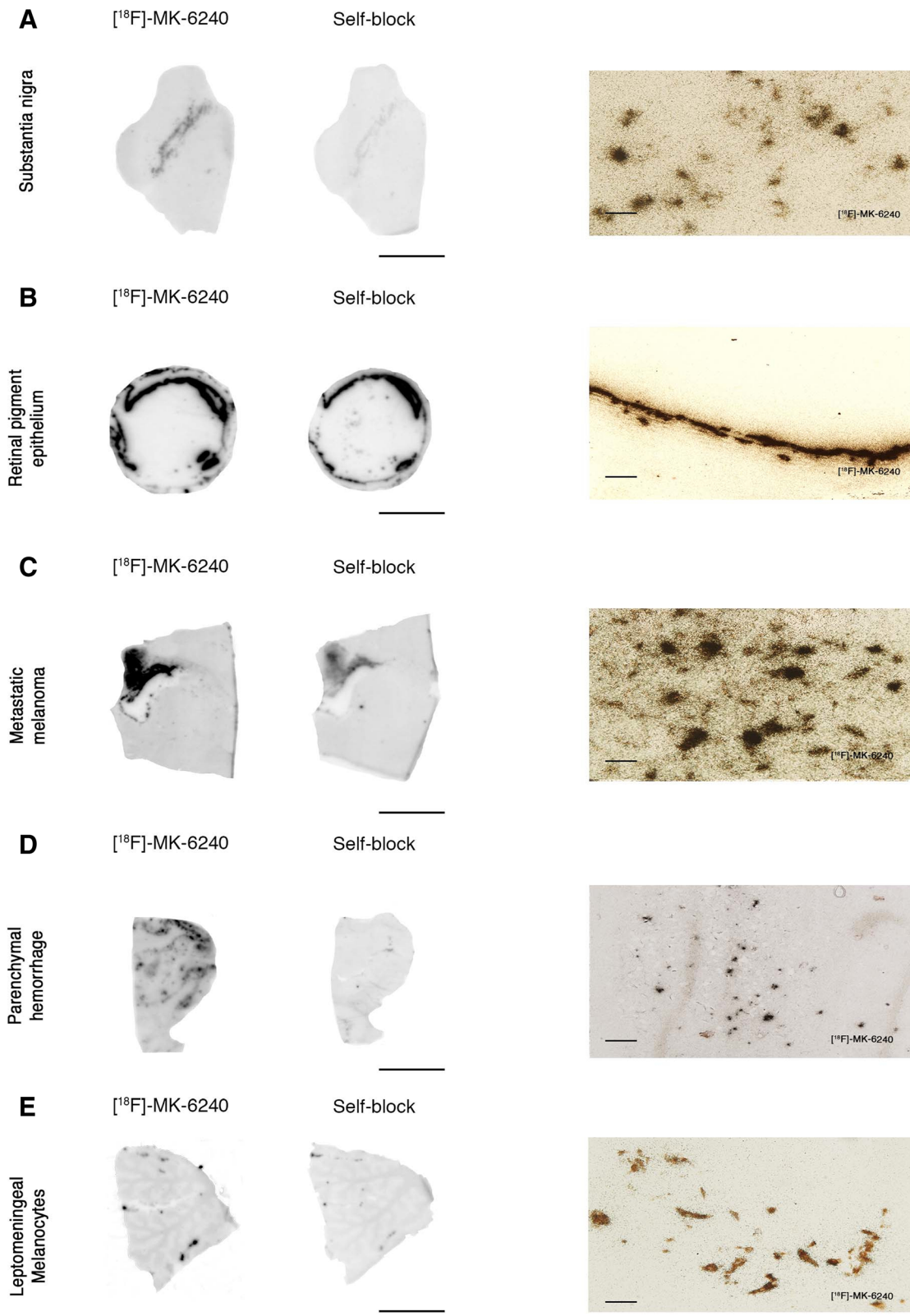


**Fig. 3** (See legend on next page.)



(See figure on previous page.)

**Fig. 3** [F-18]-MK-6240 phosphor screen and high-resolution autoradiography images of slices containing substantia nigra in a control case (#2) (a), retinal pigment epithelium (b) in an AD case (#11), metastatic melanoma (#18) (c), parenchymal hemorrhagic lesions (#43) (d) and extracutaneous meningeal melanocytes in the cerebellum of an AD case (#8) (e). [F-18]-MK-6240 phosphor screen autoradiography images are displayed in (a-e), left and middle panels. [F-18]-MK-6240 high resolution autoradiography images are displayed in (a-e), right panel. Strong [F-18]-MK-6240 binding was observed in neuromelanin-containing neurons of the substantia nigra (a), melanin containing granules in the retinal pigment epithelium (b), malignant melanocytes from a metastatic melanoma (c), and extracutaneous meningeal melanocytes (e). [F-18]-MK-6240 binding was noticed in association with intraparenchymal hemorrhagic lesions (d). Scale bars = 1 cm (a-e left and middle panels: phosphor screen autoradiography) and 50 μm (a-e right panels; high resolution nuclear emulsion autoradiography)

18]. [F-18]-MK-6240 high resolution autoradiography followed by immunostaining with PHF-1 or Aβ antibodies on the same brain slices further confirmed that the lesions labeled by the nuclear emulsion were PHF-tau aggregates, including classic NFT and PHF-tau

containing dystrophic neurites around plaques (Fig. 7a-b), but not Aβ plaques themselves (Fig. 7c) or vessels with amyloid deposits (Fig. 7d). NFT-containing slices from AD brains dipped in the nuclear photographic emulsion omitting the incubation with

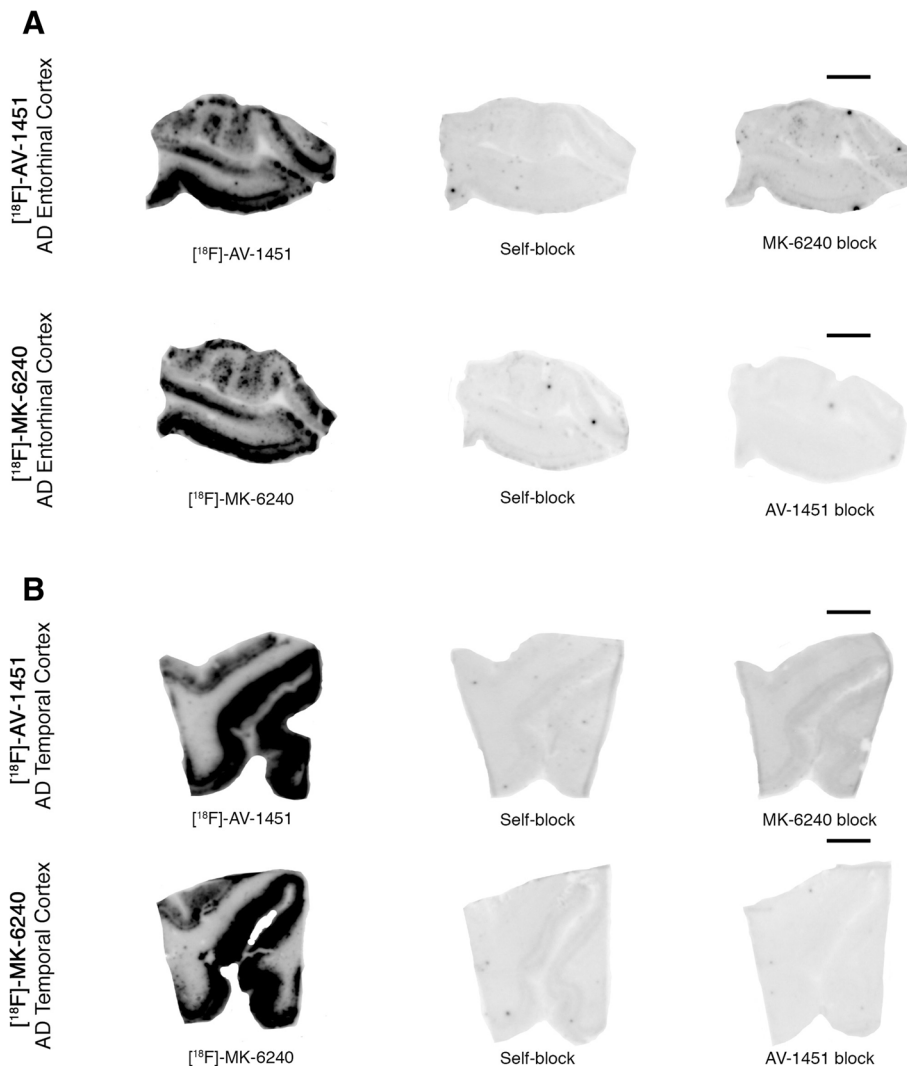
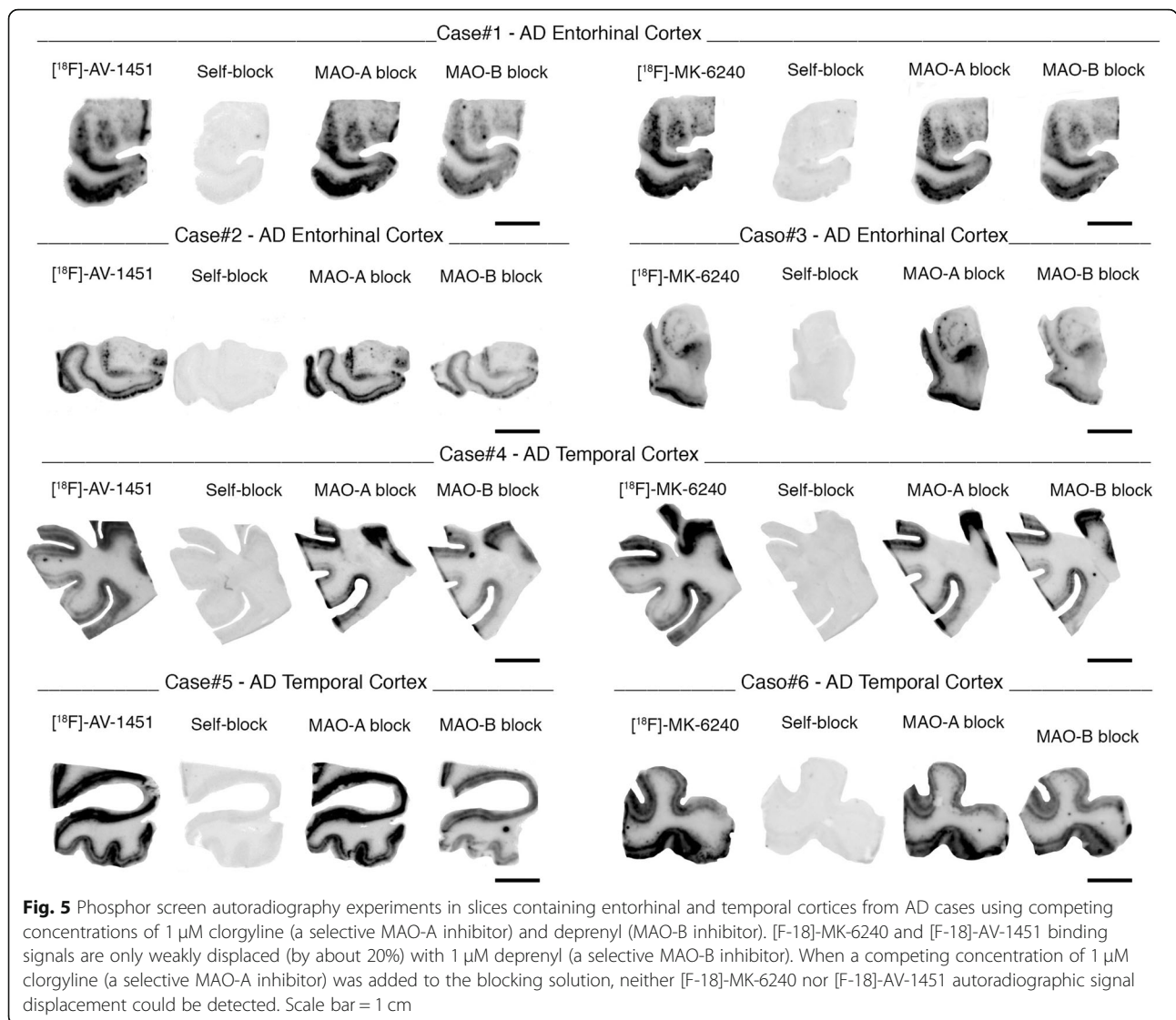


**Fig. 4** Head-to-head comparison of [F-18]-MK-6240 and [F-18]-AV-1451 phosphor screen autoradiographic binding patterns in adjacent sections obtained from the same tissue material containing entorhinal cortex (#13) (a) and superior temporal sulcus (#13) (b) from AD cases. Both tracers exhibited comparable strong binding in regions containing tangles; MK-6240 signal was blocked by adding 500 nM unlabeled AV-1451 and AV-1451 signal was almost completely blocked by adding 500 nM unlabeled MK-6240. Scale bar = 1 cm



[F-18]-MK-6240 showed no silver grain accumulation and served as negative control (not shown).

Brain slices from control brains free of tau aggregates did not show accumulation of silver grains in any of regions examined (data not shown). Negligible numbers of silver grains were observed colocalizing with tau aggregates in CTE, CBD, PSP and PiD cases (Fig. 7e-h). No silver grains were observed either colocalizing with  $\alpha$ -synuclein or TDP-43 containing inclusions (Fig. 7i-j).

Of note, neuromelanin-containing neurons in the substantia nigra pars compacta (Fig. 3a), retinal pigment epithelium (RPE) cells (Fig. 3b), tumor cells of metastatic melanoma (Fig. 3c) and leptomeningeal melanocytes (Fig. 3e), consistently demonstrated a robust concentration of silver grains confirming off-target binding of MK-6240 to neuromelanin- and melanin-containing cells. Weaker concentrations of silver grains were also observed colocalizing with parenchymal hemorrhages

(Fig. 3d), pointing to some additional [F-18]-MK-6240 off-target binding to blood components.

### Discussion

Recently multiple novel PET tracers have been reported, tailored to allow detection of tau pathology in the human living brain. The status quo is largely to use PET ligands in patients carrying a particular clinical diagnosis and then simply accept, in a somewhat circular fashion, that what the scan shows is representative of the underlying disease process. However, the correct identification of biological targets of imaging agents is an essential requirement for considering them as disease-specific and progression-specific biomarkers. Validating the underlying neuropathological binding substrate/s and identifying potential off-target binding of these novel tau ligands is critical for the accurate interpretation of their in vivo PET imaging behavior. We have carefully characterized

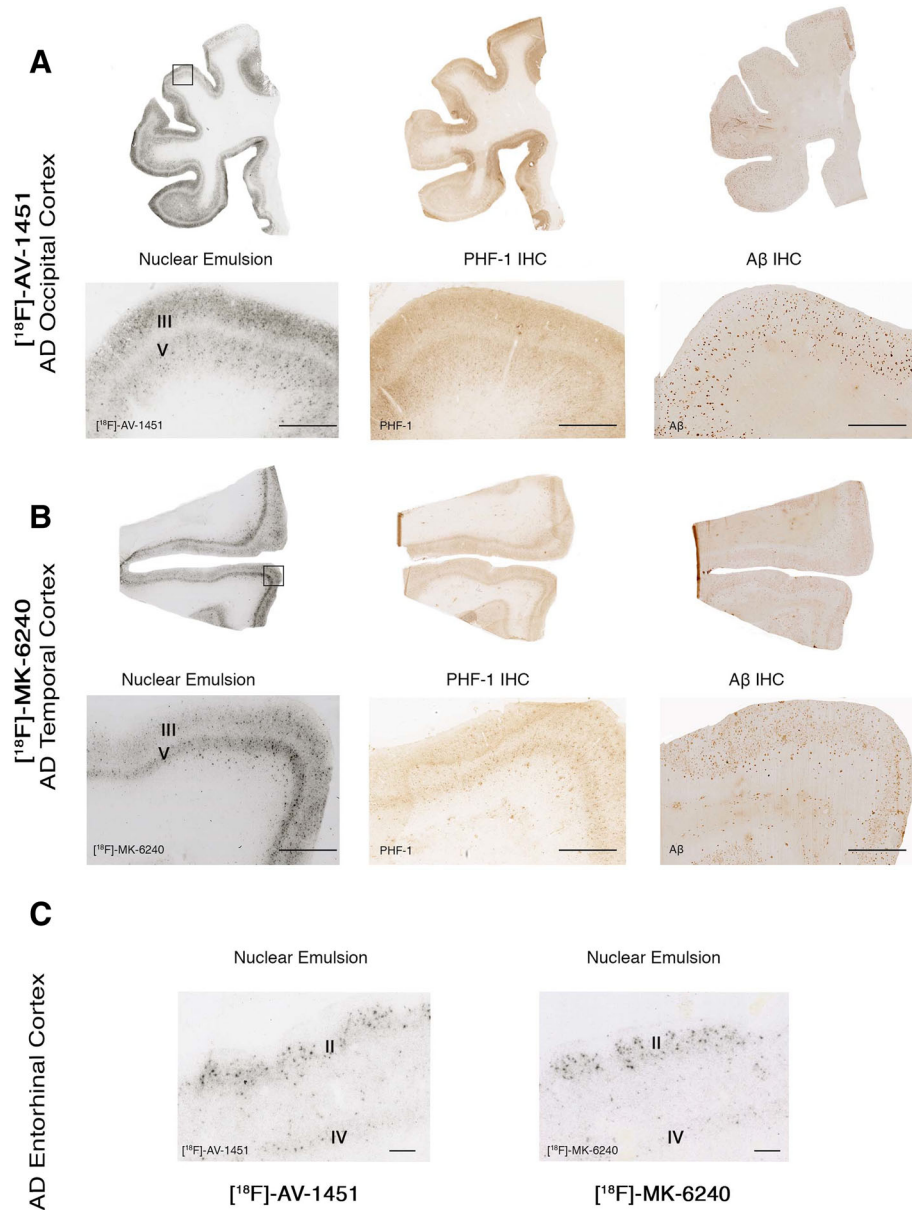


**Fig. 6**  $[^{18}\text{F}]\text{-AV-1451}$  and  $[^{18}\text{F}]\text{-MK-6240}$  phosphor screen and high resolution autoradiography photomicrographs of brain slices containing occipital (#13) **(a)**, temporal (#9) **(b)** and entorhinal (#14) **(c)** cortices from AD cases (left panels). Middle and right panels **(a and b)** show immunostaining of adjacent sections with PHF-1 antibody (kind gift of Dr. Peter Davies) and anti-A $\beta$  antibody (1:500, mouse, clone 6F/3D, Dako), respectively.  $[^{18}\text{F}]\text{-AV-1451}$  (left panels **a and c**) and  $[^{18}\text{F}]\text{-MK-6240}$  (left panel **b** and right panel **c**) high resolution nuclear emulsion autoradiography showed a strong cortical accumulation of silver grains in temporal cortical layers III and V **(a and b)**, and in layers II and IV of the entorhinal cortex **(c)** in AD brains mirroring the laminar pattern of tangles on adjacent slices as revealed by PHF-1 immunostaining (middle panels) rather than the more scattered plaque distribution pattern revealed by A $\beta$  immunostaining (right panels). Abbreviations: AD = Alzheimer’s disease; IHC = immunohistochemistry. Scale bars = 200  $\mu\text{m}$  **(a and b)** 50  $\mu\text{m}$  **(c)**

the autoradiographic binding patterns of novel tau tracer  $[^{18}\text{F}]\text{-MK-6240}$  in a collection of postmortem tissue samples representing a broad spectrum of neurodegenerative disorders. Our observations derived from combined  $[^{18}\text{F}]\text{-MK-6240}$  sensitive autoradiography and immunohistochemistry, using this compound at similar concentrations used in vivo for PET studies, indicate that

$\text{MK-6240}$  has high binding affinity for tau aggregates in AD brain tissue, but does not seem to bind to a significant extent to neuronal and glial tau aggregates in non-AD tauopathies such as PiD, PSP, CBD or CTE, or to A $\beta$ ,  $\alpha$ -synuclein or TDP-43-containing lesions. These findings strongly suggest that tau in tangles of AD has a unique conformation that is recognized by this tracer (in

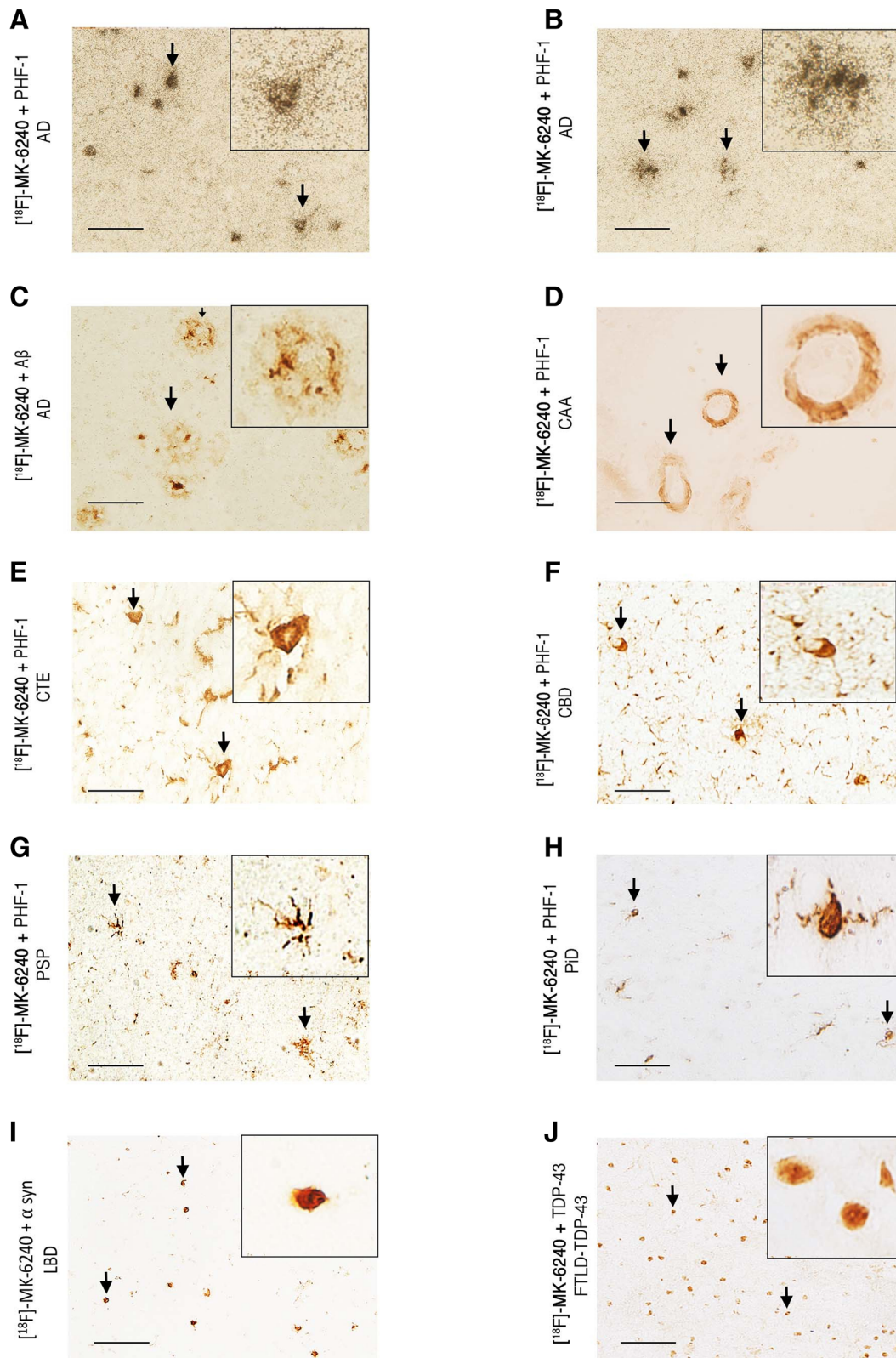


**Fig. 7** (See legend on next page.)

(See figure on previous page.)

**Fig. 7** Photomicrographs showing combined [F-18]-MK-6240 high-resolution nuclear emulsion autoradiography followed by immunostaining with appropriate antibodies of brain slices containing frontal and temporal cortices from AD (#10, #16) (a-c), CAA (#17) (d) CTE (#33) (e), CBD (#23) (f), PSP (#26) (g), PiD (#20) (h), LBD (#34) (i) and FTLD TDP-43 (#39) (j). Accumulation of silver grains from the nuclear emulsion colocalized with PHF-1 stained tangles and PHF-tau containing dystrophic neurites around plaques in AD. No detectable accumulations of silver grains were observed in association with A $\beta$  plaques themselves or amyloid-containing vessels in CAA, tau aggregates in CTE, coiled bodies and globose tangles in CBD, astrocytic plaques in PSP, Pick bodies in PiD, Lewy bodies in LBD or TDP-43 inclusions in FTLD TDP-43. Abbreviations: AD = Alzheimer's disease; CAA = cerebral amyloid angiopathy; CTE = chronic traumatic encephalopathy; CBD = corticobasal degeneration PSP = progressive supranuclear palsy; PiD = Pick's disease; LBD = Lewy body disease; FTLD TDP-43 = frontotemporal lobar degeneration with TDP-43 inclusions. Scale bar = 50  $\mu$ m

keeping with the selection process for development of this compound as a lead imaging agent). Strong binding of [F-18]-MK-6240 to neuromelanin- and melanin-containing cells and some weaker binding to brain hemorrhagic lesions was also identified, pointing to these substrates as off-target binding sites of MK-6240. Overall, [F-18]-MK-6240 autoradiographic binding patterns closely resembled those of tau PET tracer [F-18]-AV-1451. Importantly, [F-18]-MK-6240 and [F-18]-AV-1451 binding signals were only very weakly displaced using autoradiography competition with unlabeled selective MAO-B inhibitor deprenyl, suggesting that these two tracers have low binding affinity for MAO enzymes in the human brain.

MK-6240 was identified as a potential imaging agent by screening using cortical homogenates from AD tissue rich in NFT as the binding target and an amyloid plaque tracer for counter-screen [15]. Based on this, we anticipated that MK-6240 would preferentially bind to tau lesions in the form of NFT in AD over other tau aggregates in non-AD tauopathies or lesions primarily made of A $\beta$ ,  $\alpha$ -synuclein or TDP-43. To date, only very limited data from human in vivo [F-18]-MK-6240 PET imaging studies have been published [2, 19]. Results from these early studies point to a promising 2- to 3-fold higher in vivo [F-18]-MK-6240 retention in neocortical and medial temporal brain regions of AD patients compared to elderly cognitively normal individuals [19]. Because this ligand is already being incorporated into clinical trial research, validation studies such as this paper are absolutely critical to evaluate the potential usefulness of this ligand as a reliable marker of human brain tau lesions. In an attempt to advance towards that goal, we applied [F-18]-MK-6240 phosphor screen and high resolution autoradiography to the study of a series of autopsy samples from individuals with a definitive diagnosis of AD, PiD, PSP, CBD, CTE, CAA, FTLD-TDP-43, DLB, and control brains free of neurodegenerative pathology. Our results confirmed that while [F-18]-MK-6240 avidly bound to PHF-tangle containing slices from AD brains, it did not bind to a significant extent to tau-containing lesions in slices from non-AD tauopathy brains, suggesting that this tracer has higher affinity and selectivity for PHF-tau over tau aggregates

with a primarily straight filament ultrastructure, and thus raising reasonable doubts about the potential value of this ligand as a biomarker of tau pathology in non-AD tauopathies. The regional and laminar autoradiographic patterns of distribution of [F-18]-MK-6240, as revealed by the combination of autoradiography using a fine grain nuclear emulsion and immunohistochemistry, closely matched those of classic PHF-tangles in AD brains [1, 18]. Using this method, we confirmed that [F-18]-MK-6240-labeled lesions were NFT, suggesting that these lesions are the main pathological substrate of [F-18]-MK-6240 binding. The microscopic examination of diffuse plaques, CAA,  $\alpha$ -synuclein and TDP-43 aggregates confirmed the absence of detectable [F-18]-MK-6240 binding to these lesions, favoring the relative selectivity of [F-18]-MK-6240 for NFT over  $\beta$ -amyloid plaques and other abnormal protein aggregates with a  $\beta$ -pleated sheet conformation.

Our data also establish that MK-6240 is not fully selective for PHF-tau deposits. Similarly to AV-1451, MK-6240 exhibits strong off-target binding to neuromelanin- and melanin-containing cells including pigmented neurons in the substantia nigra (regardless of the presence or absence of nigral tau pathology), leptomeningeal melanocytes, metastatic melanoma and retinal pigment epithelium, with some weaker off-target binding to brain hemorrhages as well. This is something relevant for the correct interpretation of [F-18]-MK-6240 in vivo imaging depending for example on the relative abundance and distribution of leptomeningeal melanocytes across different individuals [10], the possibility of focal artifactual increases in the density of these cells due to regional cortical atrophy, or the presence of concomitant brain hemorrhagic lesions.

One of the first generation tau PET tracers, THK-5351, has been recently found to demonstrate high binding affinity to MAO-B [13, 24], seriously compromising its value as a tau-specific tracer and increasing the need for alternative tau-specific imaging agents. To date, studies on potential non-specific binding of AV-1451 to MAO enzymes are scarce and have yielded conflicting results. A recent study by Vermeiren and colleagues suggested that H3-AV-1451 binds with similar nanomolar affinity to tau fibrils and MAO-A and B enzymes in

brain homogenates isolated from AD or PSP patients as well as those devoid of tau pathology [30]. Merck's researchers also reported high affinity displacement of 3H-AV-1451 binding, but not of 3H-MK-6240, in some non-AD brain homogenates in the presence of selective MAO-A inhibitor clorgyline. By contrary, Hansen and colleagues found that MAO-B inhibitors did not block in vivo [F-18]-AV-1451 binding in a series of 16 of 27 PD patients receiving MAO-B inhibitors at the time of scan [12]. In agreement with these results, Lemoine et al. reported that AV-1451 shows ten times lower affinity to MAO-B when compared to THK-5351 in in vitro assays [17]. Consistent with these observations, our data derived from [F-18]-MK-6240 and [F-18]-AV-1451 autoradiography experiments in the presence of selective MAO-A and MAO-B inhibitors point to a low binding affinity of both tracers for MAO enzymes. Studies using the specific enzymatic inhibitors do not exclude interaction of MK-6240 with MAO isoforms at regions removed from the active site. The discrepancies among the different studies could stem from the different techniques and isotope labeling used in each case e.g. in vitro binding assays in brain homogenates vs. autoradiography assays in tissue slices, and labeling of the tau tracer with H-3 vs. F-18. Our previous experience with H-3-AV-1451 in vitro binding assays in brain homogenates suggested that the signal-to background noise ratio when using this method was relatively low compared to [F-18]-AV-1451 autoradiographic techniques; something that could be due, at least in part, to off-target binding to sample components such as blood.

## Conclusions

In conclusion, all together our results show that MK-6240 exhibits a nearly identical binding profile to AV-1451 holding promise as a potential surrogate marker for the in vivo detection of neurofibrillary tangles in AD, while still having various forms of off-target binding that need to be considered when interpreting in vivo imaging findings. The utility of MK-6240 for the reliable in vivo detection of tau aggregates in non-AD tauopathies, however, seems very limited. Both, MK-6240 and AV-1451, as opposed to other tracers like THK-5351, seem to exhibit relatively low binding affinity for MAO enzymes. Future imaging-pathological correlation studies on postmortem material from patients scanned while alive will provide additional information on the utility of these two tracers for the reliable quantification of NFT burden in AD and disease progression tracking by in vivo neuroimaging, as well as their potential usefulness when testing therapeutic approaches aimed at decreasing or halting the progression of tau aggregation in AD.

## Availability of data and materials

Original slides and diagnostic material are retained. There are no novel reagents or materials for others to request.

## Authors' contributions

CA participated in study design, carried out immunostaining, phosphor screen and nuclear emulsion autoradiography, data analysis and drafted the manuscript. MD carried out phosphor screen autoradiography. MDN participated in study design, analysis and interpretation of data and carried out phosphor screen autoradiography. ACA carried out immunostaining and tissue cryosectioning. NJG participated in phosphor screen autoradiography. RN carried out radiotracer synthesis and labeling. MM carried out immunostaining and tissue cryosectioning. GEF participated in study design, analysis and interpretation of data. KAJ participated in the study design. MPF carried out the neuropathologic examination and participated in the study design, analysis and interpretation of data. TGI conceived the study and participated in its design and coordination, analysis and interpretation of data and drafted the manuscript. All authors read and approved the final manuscript.

## Ethics approval and consent to participate

All procedures performed in studies involving human participants were in accordance with the ethical standards of the institutional and national research committee and with the 1964 Helsinki declaration and its later amendments.

## Consent for publication

Informed consent was obtained from all individual participants included in the study and according to institutional procedures for autopsy consents for post-mortem tissue.

## Competing interests

Cynthia Agüero received research funding from the International Health Central America Institute, San Jose, Costa Rica. Marc D. Normandin received research funding from NIH National Institute of Neurological Disorders and Stroke (U01NS086659) and NIH National Institute of Mental Health (R01MH100350). Keith A. Johnson received research funding from NIH (grants R01 EB014894, R21 AG038994, R01 AG026484, R01 AG034556, P50 AG00513421, U19 AG10483, P01 AG036694, R13 AG042201174210, R01 AG027435 and R01 AG037497) and the Alzheimer's Association (ZEN-10-174,210 K). Keith A. Johnson has served as paid consultant for Bayer, GE Healthcare, Janssen Alzheimer's Immunotherapy, Siemens Medical Solutions, Genzyme, Novartis, Biogen, Roche, ISIS Pharma, AZTherapy, GEHC, Lundberg, and Abbvie. He is a site co-investigator for Lilly/Avid, Janssen Immunotherapy and Pfizer. Matthew P. Frosch received research funding from the Massachusetts Alzheimer's Disease Research Center (NIH AG005134). Teresa Gómez-Isla received research funding from NIH National Institute on Aging (AG005134, AG036694 and AG061206). Teresa Gómez-Isla participated as speaker in an Eli Lilly and Company sponsored educational symposium and serves in an Eli Lilly Data Monitoring Committee. Eli Lilly and Company owns Avid, the company that created AV-1451, one of the PET compounds used in this study.

## Publisher's Note

Springer Nature remains neutral with regard to jurisdictional claims in published maps and institutional affiliations.

## Author details

<sup>1</sup>Department of Neurology, Massachusetts General Hospital, WACC, Suite 715, 15th Parkman St., Boston, MA 02114, USA. <sup>2</sup>MassGeneral Institute for Neurodegenerative Disease, Charlestown, MA, USA. <sup>3</sup>Center for Advanced Medical Imaging Sciences, Division of Nuclear Medicine and Molecular Imaging, Department of Radiology, Massachusetts General Hospital, Harvard Medical School, Boston, MA, USA. <sup>4</sup>AP-HP, Department of Nuclear Medicine, Pitié-Salpêtrière Hospital, Sorbonne University, UPMC Paris 06, CNRS UMR 7371, INSERM U1146, 75013 Paris, France. <sup>5</sup>Department of Radiology, Massachusetts General Hospital, Boston, MA, USA. <sup>6</sup>C.S. Kubik Laboratory for Neuropathology, Massachusetts General Hospital, Boston, MA, USA.

Received: 21 February 2019 Accepted: 23 February 2019

Published online: 11 March 2019

## References

1. Arnold SE, Hyman BT, Flory J, Damasio AR, Van Hoesen GW (1991) The topographical and neuroanatomical distribution of neurofibrillary tangles

- and neuritic plaques in the cerebral cortex of patients with Alzheimer's disease. *Cereb Cortex* 1:103–116
2. Betthausen TJ, Cody KA, Zammit MD, Murali D, Converse AK, Barnhart TE, Stone CK, Rowley HA, Johnson SC, Christian BT (2018) In vivo characterization and quantification of neurofibrillary tau PET radioligand [(18F)MK-6240 in humans from Alzheimer's disease dementia to young controls. *J Nucl Med*. <https://doi.org/10.2967/jnumed.118.209650>. Epub ahead of print. PubMed PMID: 29777006.
  3. Braak H, Alafuzoff I, Arzberger T, Kretschmar H, Del Tredici K (2006) Staging of Alzheimer disease-associated neurofibrillary pathology using paraffin sections and immunocytochemistry. *Acta Neuropathol* 112:389–404
  4. Brier MR, Gordon B, Friedrichsen K, McCarthy J, Stern A, Christensen J, Owen C, Aldea P, Su Y, Hassenstab J, Cairns NJ, Holtzman DM, Fagan AM, Morris JC, Benzinger TLS, Ances BM (2016) Tau and ab imaging, CSF measures, and cognition in Alzheimer's disease. *Sci Transl Med* 8:1–9
  5. Caro LG, Van Tubergen RP, Kolb JA (1962) High-resolution autoradiography. *J Cell Biol* 15:173–188
  6. Cho H, Choi JY, Hwang MS, Kim YJ, Lee HM, Lee HS, Lee JH, Ryu YH, Lee MS, Lyoo CH (2016a) In vivo cortical spreading pattern of tau and amyloid in the Alzheimer disease spectrum. *Ann Neurol* 80:247–258
  7. Cho H, Choi JY, Hwang MS, Lee JH, Kim YJ, Lee HM, Lyoo CH, Ryu YH, Lee MS (2016b) Tau PET in Alzheimer disease and mild cognitive impairment. *Neurology* 87:375–383
  8. Collier TL, Yokell DL, Livni E, Rice PA, Celen S, Serdons K, Neelamegam R, Bormans G, Harris D, Walji A, Hostetler ED, Bennacef I, Vasdev N (2017) cGMP production of the radiopharmaceutical [(18) F]MK-6240 for PET imaging of human neurofibrillary tangles. *J Labelled Comp Radiopharm* 60: 263–269
  9. Gerfen CR (2003) Basic neuroanatomical methods. *Curr Protoc Neurosci* Chapter 1:Unit 1.1
  10. Goldgeier MH, Klein LE, Klein-Angerer S, Moellmann G, Nordlund JJ (1984) The distribution of melanocytes in the Leptomeninges of the human brain. *J Invest Dermatol* 82:235–238
  11. Gordon BA, Friedrichsen K, Brier M, Blazey T, Su Y, Christensen J, Aldea P, McConathy J, Holtzman DM, Cairns NJ, Morris JC, Fagan AM, Ances BM, Benzinger TL (2016) The relationship between cerebrospinal fluid markers of Alzheimer pathology and positron emission tomography tau imaging. *Brain* 139:2249–2260
  12. Hansen AK, Brooks DJ, Borghammer P (2017) MAO-B Inhibitors Do Not Block In Vivo Flortaucipir([(18)F]-AV-1451) Binding. *Mol Imaging Biol* 20:356–360
  13. Harada R, Furumoto S, Tago T, Furukawa K, Ishiki A, Tomita N, Iwata R, Tashiro M, Arai H, Yanai K, Kudo Y, Okamura N (2016) Characterization of the radiolabeled metabolite of tau PET tracer (18)F-THK5351. *Eur J Nucl Med Mol Imaging* 43:2211–2218
  14. Hong M, Zhukareva V, Vogelsberg-Ragaglia V, Wszolek Z, Reed L, Miller BI, Geschwind DH, Bird TD, McKeel D, Goate A, Morris JC, Wilhelmsen KC, Schellenberg GD, Trojanowski JQ, Lee VM-Y (1998) Mutation-specific functional impairments in distinct tau isoforms of hereditary FTDP-17. *Science* 282:1914–1917
  15. Hostetler ED, Walji AM, Zeng Z, Miller P, Bennacef I, Salinas C, Connolly B, Gantert L, Haley H, Holahan M, Purcell M, Riffel K, Lohith TG, Coleman P, Soriano A, Ogawa A, Xu S, Zhang X, Joshi E, Della Rocca J, Hesk D, Schenk DJ, Evelhoch JL (2016) Preclinical characterization of 18F-MK-6240, a promising PET tracer for in vivo quantification of human neurofibrillary tangles. *J Nucl Med* 57:1599–1606
  16. Johnson KA, Schultz A, Betensky RA, Becker JA, Sepulcre J, Rentz D, Mormino E, Chhatwal J, Amariglio R, Papp K, Marshall G, Albers M, Mauro S, Pepin L, Alverio J, Judge K, Philiosaint M, Shoup T, Yokell D, Dickerson B, Gomez-Isla T, Hyman B, Vasdev N, Sperling R (2016) Tau positron emission tomographic imaging in aging and early Alzheimer disease. *Ann Neurol* 79: 110–119
  17. Lemoine L, Gillberg PG, Svedberg M, Stepanov V, Jia Z, Huang J, Nag S, Tian H, Ghetti B, Okamura N, Higuchi M, Halldin C, Nordberg A (2017) Comparative binding properties of the tau PET tracers THK5117, THK5351, PBB3, and T807 in postmortem Alzheimer brains. *Alzheimers Res Ther* 9:96
  18. Lewis DA, Campbell MJ, Terry RD, Morrison JH (1987) Laminar and regional distributions of neurofibrillary tangles and neuritic plaques in Alzheimer's disease: a quantitative study of visual and auditory cortices. *J Neurosci* 7: 1799–1808
  19. Lohith TG, Bennacef I, Vandenberghe R, Vandenbulcke M, Salinas-Valenzuela C, Declercq R, Reynders T, Telan-Choing F, Riffel K, Celen S, Serdons K, Bormans G, Tsai K, Walji A, Hostetler ED, Evelhoch JL, Van Laere K, Forman M, Stoch A, Sur C, Struyk A (2018) First-in-human brain imaging of Alzheimer dementia patients and elderly controls with (18)F-MK-6240, a PET tracer targeting neurofibrillary tangle pathology. *J Nucl Med*. <https://doi.org/10.2967/jnumed.118.208215> [Epub ahead of print] PubMed PMID: 29880509
  20. Lowe VJ, Curran G, Fang P, Liesinger AM, Josephs KA, Parisi JE, Kantarci K, Boeve BF, Pandey MK, Bruinsma T, Knopman DS, Jones DT, Petrucelli L, Cook CN, Graff-Radford NR, Dickson DW, Petersen RC, Jack CR Jr, Murray ME (2016) An autoradiographic evaluation of AV-1451 tau PET in dementia. *Acta Neuropathol Commun* 4:58
  21. Marquie M, Normandin MD, Meltzer AC, Siao Tick Chong M, Andrea NV, Anton-Fernandez A, Klunk WE, Mathis CA, Ikonomic MD, Debnath M, Bien EA, Vandenberg CR, Costantino I, Makarets S, DeVos SL, Oakley DH, Gomperts SN, Growdon JH, Domoto-Reilly K, Lucente D, Dickerson BC, Frosch MP, Hyman BT, Johnson KA, Gomez-Isla T (2017) Pathological correlations of [F-18]-AV-1451 imaging in non-alzheimer tauopathies. *Ann Neurol* 81:117–128
  22. Marquie M, Normandin MD, Vandenberg CR, Costantino IM, Bien EA, Rycyna LG, Klunk WE, Mathis CA, Ikonomic MD, Debnath ML, Vasdev N, Dickerson BC, Gomperts SN, Growdon JH, Johnson KA, Frosch MP, Hyman BT, Gomez-Isla T (2015) Validating novel tau positron emission tomography tracer [F-18]-AV-1451 (T807) on postmortem brain tissue. *Ann Neurol* 78:787–800
  23. McKee AC, Stern RA, Nowinski CJ, Stein TD, Alvarez VE, Daneshvar DH, Lee HS, Wojtowicz SM, Hall G, Baugh CM, Riley DO, Kubilus CA, Cormier KA, Jacobs MA, Martin BR, Abraham CR, Ikezu T, Reichard RR, Wolozin BL, Budson AE, Goldstein LE, Kowall NW, Cantu RC (2013) The spectrum of disease in chronic traumatic encephalopathy. *Brain* 136:43–64
  24. Ng KP, Pascoal TA, Mathotaarachchi S, Theriault J, Kang MS, Shin M, Guiot MC, Guo Q, Harada R, Comley RA, Massarweh G, Soucy JP, Okamura N, Gauthier S, Rosa-Neto P (2017) Monoamine oxidase B inhibitor, selegiline, reduces (18)F-THK5351 uptake in the human brain. *Alzheimers Res Ther* 9:25
  25. Pontecorvo MJ, Devous MD Sr, Navitsky M, Lu M, Salloway S, Schaerf FW, Jennings D, Arora AK, McGeehan A, Lim NC, Xiong H, Joshi AD, Siderowf A, Mintun MA (2017) Relationships between flortaucipir PET tau binding and amyloid burden, clinical diagnosis, age and cognition. *Brain* 140:748–763
  26. Reed LA, Grabowski TJ, Schmidt ML, Morris JC, Goate A, Solodkin A, Van Hoesen GW, Schelper RL, Talbot CJ, Wragg MA, Trojanowski JQ (1997) Autosomal dominant dementia with widespread neurofibrillary tangles. *Ann Neurol* 42(4):564–572
  27. Sander K, Lashley T, Gami P, Gendron T, Lythgoe MF, Rohrer JD, Schott JM, Revesz T, Fox NC, Arstad E (2016) Characterization of tau positron emission tomography tracer [(18)F]AV-1451 binding to postmortem tissue in Alzheimer's disease, primary tauopathies, and other dementias. *Alzheimers Dement* 12:1116–1124
  28. Scholl M, Lockhart SN, Schonhaut DR, O'Neil JP, Janabi M, Ossenkoppele R, Baker SL, Vogel JW, Faria J, Schwimmer HD, Rabinovici GD, Jagust WJ (2016) PET imaging of tau deposition in the aging human brain. *Neuron* 89:971–982
  29. Van Nostrand WE, Melchor JP, Cho HS, Greenberg SM, Rebeck GW (2001) Pathogenic effects of D23N Iowa mutant amyloid beta-protein. *J Biol Chem* 276: 32860–32866
  30. Vermeiren C, Motte P, Viot D, Mairet-Coello G, Courade JP, Citron M, Mercier J, Hannestad J, Gillard M (2017) The tau positron-emission tomography tracer AV-1451 binds with similar affinities to tau fibrils and monoamine oxidases. *Mov Disord* 33:273–281
  31. Vonsattel JP, Amaya Mdel P, Cortes EP, Mancevska K, Keller CE (2008) Twenty-first century brain banking: practical prerequisites and lessons from the past: the experience of New York Brain Bank, Taub Institute, Columbia University. *Cell Tissue Bank* 9:247–258
  32. Walji AM, Hostetler ED, Selnick H, Zeng Z, Miller P, Bennacef I, Salinas C, Connolly B, Gantert L, Holahan M, O'Malley S, Purcell M, Riffel K, Li J, Balsells J, O'Brien JA, Melquist S, Soriano A, Zhang X, Ogawa A, Xu S, Joshi E, Della Rocca J, Hess FJ, Schachter J, Hesk D, Schenk D, Struyk A, Babaoglu K, Lohith TG, Wang Y, Yang K, Fu J, Evelhoch JL, Coleman PJ (2016) Discovery of 6-(Fluoro-(18)F)-3-(1H-pyrrolo[2,3-c]pyridin-1-yl)isoquinolin-5-amine [(18)F]-MK-6240: a positron emission tomography (PET) imaging agent for quantification of neurofibrillary tangles (NFTs). *J Med Chem* 59:4778–4789
  33. Wang L, Benzinger TL, Su Y, Christensen J, Friedrichsen K, Aldea P, McConathy J, Cairns NJ, Fagan AM, Morris JC, Ances BM (2016) Evaluation of tau imaging in staging Alzheimer disease and revealing interactions between beta-amyloid and Tauopathy. *JAMA Neurol* 73: 1070–1077

34. Woodbury DH, Beierwaltes WH (1967) Fluorine-18 uptake and localization in soft tissue deposits of osteogenic sarcoma in rat and man. *J Nucl Med* 8: 646–651
35. Xia CF, Arteaga J, Chen G, Gangadharmath U, Gomez LF, Kasi D, Lam C, Liang Q, Liu C, Mocharla VP, Mu F, Sinha A, Su H, Szardenings AK, Walsh JC, Wang E, Yu C, Zhang W, Zhao T, Kolb HC (2013) [(18)F]T807, a novel tau positron emission tomography imaging agent for Alzheimer's disease. *Alzheimers Dement* 9:666–676

**Ready to submit your research? Choose BMC and benefit from:**

- fast, convenient online submission
- thorough peer review by experienced researchers in your field
- rapid publication on acceptance
- support for research data, including large and complex data types
- gold Open Access which fosters wider collaboration and increased citations
- maximum visibility for your research: over 100M website views per year

**At BMC, research is always in progress.**

Learn more [biomedcentral.com/submissions](https://biomedcentral.com/submissions)

